Apparent colossal dielectric constants in nanoporous Metal Organic Frameworks

*M. Sánchez-Andújar, S. Yáñez-Vilar, B. Pato-Doldán, C. Gómez-Aguirre, S. Castro-García, M. A. Señarís-Rodríguez**

Department of Fundamental Chemistry, Faculty de Sciences, University of A Coruña, Campus A Coruña, 15071 A Coruna, Spain

**Fax: +34981167065; Tel: +34981167000 e-mail: m.senaris.rodriguez@udc.es*

In this work, we show that the hybrid material $Co_2(1,4\text{-bdc})_2(dabco)\cdot[4DMF\cdot 1H_2O]$, shows an apparent colossal dielectric constant at room temperature ($\varepsilon'_r \approx 5000$ at 300 K for ν=100 Hz). Nevertheless, such response does not imply colossal polarizability processes, as its dielectric constant is not purely intrinsic, but is greatly enhanced by the activation of extrinsic dielectric effects close to room temperature associated to the diffusion of numerous guest molecules through the channels. If such extrinsic contributions are eliminated or reduced, the values of the dielectric constant turn to be much smaller, as observed in the closely related $Co_2(1,4\text{-bdc-}NH_2)_2(dabco)\cdot[7/2DMF\cdot 1H_2O]$, $Co_2(1,4\text{-ndc})_2(dabco)\cdot[3DMF\cdot 2H_2O]$ and $Ni_2(1,4\text{-bdc})_2(dabco)\cdot[3DMF\cdot 1/2H_2O]$ compounds. Therefore, we warn about the imperious necessity of distinguishing between intrinsic and extrinsic effects in electrically inhomogenous MOF materials that display a certain conductivity in order to adequately interpret their dielectric behavior.

KEYWORDS: *Metal organic frameworks, dielectric properties, extrinsic contributions.*

INTRODUCTION

Hybrid materials consisting of metal atoms or clusters that are linked by polyfunctional organic ligands forming one-, two-, or three-dimensional structures that can be nanoporous –the so-called metal organic frameworks MOFs– have been extensively studied in the last decade in view of their interesting potential applications, for example, in catalysis and gas storage.[1] In addition they are receiving increasing attention as they can display a wide range of interesting functional properties[2] among them, and as very recently found, dielectric[3] and even multiferroic properties.[2c,4,5]

In this new search for dielectric hybrids, a very interesting possibility is the appearance of electrical order or dielectric anomalies induced by order-disorder processes of polar and/or H-bonded guest molecules allocated in cavities of host structures.[3]

Such a behavior has been found, for example, in alkylamonium transition metal formates such as $[(CH_3)_2NH_2][M(HCOO)_3]$ (M^{2+}=Zn^{2+}, Mn^{2+}, Co^{2+}, etc.).[5,6] These are dense MOFs with perovskite structure, where a cooperative ordering[5,6a] or freezing[6b] of the guest species leads to a remarkable dielectric transition in the range 160-185 K depending on the specific metal.[5,6]

Very interestingly, some MOFs that contain interconnected nanopores (tunnels) where movable polar molecules are loosely bound have also been reported to show interesting dielectric behavior.[7-10] Nevertheless an important limitation is that their very porous structure facilitates the evaporation or loss of the guest species on approaching room temperature, thus preventing in many cases from obtaining good and reliable dielectric responses in this temperature window.[8-11] If such elimination is avoided, for example by encapsulating the samples in Teflon-sealed cylindrical cells during the dielectric measurements[12], very large dielectric constants can be observed at room temperature or above.

For example, the compound $[Sm_2Cu_3(IDA)_6]\cdot 9H_2O$ (where IDA: iminodiacetate) has been reported to display a very large dielectric constant, $\varepsilon'_{r,max} \approx 1300$ at T=400 K and peculiar hysteresis loops.[11] Such dielectric behavior has been explained on the basis of local thermal motion of water molecules confined in the tunnels, together with an additional antiferroelectric order that would take place at 350 K.[11]

In the same context, the hybrid $\{(EMI)_2[Zn_3(1,2,4,5\text{-}BTC)_2]2H_2O\}_n$ (where EMI: 1-ethyl-3-methyl imidazolium and BTC: benzenetetracarboxylate) compound has been reported to display a very high dielectric constant $\varepsilon'_r \approx 5 \cdot 10^6$ at 100 Hz, that decreases various orders of magnitude as frequency increases. This compound, that at difference with the previous case is non-centrosymmetric, also displays an anomalous P(E) curve, and has been described as ferroelectric.[13]

Taken into account that dielectric constant values $\varepsilon'_r > 10^3$ are considered "colossal",[14] these hybrid compounds would then belong to the outstanding and desired group of colossal dielectric constant (CDC) materials.

Apart from the obvious technical importance of CDCs for applications that require high ε'_r electronic materials, a key issue from the scientific point of view is the microscopic origin of such a behavior. That is, whether such dielectric response is really intrinsic from the bulk material, and thus is based on colossal polarizability processes, or if it is in fact a combination of intrinsic and extrinsic contributions that give rise to the observed macroscopic behavior.

Such a question of intrinsic *versus* apparent CDCs is not new, but has in fact been at the center of an intense and extended debate and discussion in other fields of Solid State and Materials Science. In this regard it is worth recalling the recent and very fruitful debate and controversy [15] about CDC oxides such as $CaCu_3Ti_4O_{12}$ [16,17] or $CaMn_7O_{12}$ [18] that display dielectric constants of $\sim 1 \cdot 10^6$ at 1 kHz and at 300 K. After strong discussion, it is now widely accepted that these oxides are in fact electrically heterogeneous materials, where Maxwell-Wagner polarization effects (arising from the presence of a certain electronic conductivity, formation of Schottky-like electrodes, etc.)[19] markedly enhance the values of their dielectric constants. Or the case of biological materials, that also show very large ε'_r at low frequencies, not because their are ferroelectric but because they are electrically inhomogeneous and good ionic conductors due to its water content, resulting in an accumulation of electrical charge close to the contacts. [20]

Both types of polarization effects, that give rise to a substantial magnification of the materials capacitance, are in fact exploited in practical applications such as in barrier layer capacitors [21] and in supercapacitors, [22] respectively.

In view of such a background, and using our previous experience in the study of the dielectric properties of mixed oxides with high dielectric constants, we have carried out the present work with a twofold purpose: 1/ to clarify the real origin of the colossal dielectric constants that can be measured on MOF materials; 2/ to warn about the necessity of distinguishing between intrinsic and extrinsic effects to correctly interpret their dielectric behavior.

For this purpose, we have searched in the literature for inclusion MOF compounds that display "medium" size 3D cavities, that is: cavities that are sufficiently large to allow the presence of several guest species with considerable degree of freedom, but small enough to prevent their easy loss at room temperature (to ensure that the compounds are fairly stable towards the loss of the included molecules).

Our choice has been nanoporous MOFs of formula $M_2(1,4\text{-bdc})_2(dabco)\cdot[G]$ (M^{2+}= Co^{2+} or Ni^{2+}; *1,4-bdc*= 1,4- benzenedicarboxylate anions, *dabco*= 1,4-diazabicyclo[2.2.2]octane and G= DMF and H_2O, DMF= N,N-dimethylformamide), whose synthesis, room temperature crystal structure and adsorption properties has been previously reported [23] even if not their dielectric behavior.

From the structural point of view, the framework of these compounds consists of two-dimensional layers of M_2-paddle wheels that are linked together by *1,4-bdc* anions while *dabco* molecules act as pillar ligands that connect the square nets into a 3D host structure (Fig. 1).[24]

Such framework displays a 3D interconnected pore system[25] where several polar guest species are located (namely 4 DMF and 1 H_2O in the case of the Co compound). Very interestingly, such guest molecules can be removed from the compound by appropriate heating treatments without altering its 3D architecture.[25]

In addition, we have extended these studies to the derivative compounds $Co_2(L)_2(dabco)\cdot[G]$ whose structures are closely related to this one, but where the *1,4-bdc* ligand is either replaced by the NH_2-substituted *1,4-bdc* ligand (*1,4-bdc-NH_2*) or by the benzene-functionalized ligand *1,4-ndc* (*1,4-ndc*: 1,4-

naphthalenedicarboxylate anion), (see Fig. S1 of Supporting Information S.I.). The interest of these substitutions is that the presence of the phenyl and amine groups reduces considerably the aperture size of the pores.[26]

EXPERIMENTAL

Synthesis

The $Co_2(L)_2(dabco)\cdot[G]$ compounds (M= Co^{2+}, Ni^{2+}; L= *1,4-bdc*, *1,4-bdc-NH$_2$*, *1,4-ndc*) were synthesized according to the procedure described in the literature.[23,2¡Error! Marcador no definido.5] In a typical experiment, 2.5 mmol of $M(NO_3)_2\cdot 6H_2O$ and 2.5 mmol of H_2bdc, H_2bdc-NH_2 or H_2ndc were initially dissolved in 30 mL of DMF, to which 1.25 mmol of *dabco* were subsequently added.

For the synthesis of $Co_2(1,4\text{-bdc})_2(dabco)\cdot[G]$ (compound **1**) and $Ni_2(1,4\text{-bdc})_2(dabco)\cdot[G]$ (compound **2**), the resulting solutions were heated in Teflon-lined autoclaves at 403 K during 60 hours and, after slow overnight cooling, the obtained products were collected, washed with DMF, and dried at room temperature. The samples were then stored in desiccators to ensure removal of any solvent molecules which could remain adsorbed on the surface of the particles.

The synthesis of $Co_2(1,4\text{-bdc-}NH_2)_2(dabco)\cdot[G]$ (compound **3**) and $Co_2(1,4\text{-ndc})_2(dabco)\cdot[G]$ (compound **4**) were carried out as follows: the initial reactants were stirred at room temperature for 3 hours; the clear solutions obtained after the removal of residual precipitates were heated in sealed glass tubes at 393 K for 65 hours (compound **3**) or in Teflon-lined autoclaves at 393 K during 72 hours (compound **4)**. The obtained crystals were collected, washed with DMF, dried at room temperature and stored in desiccators in order to remove any solvent which could remain adsorbed on the surface and avoid the adsorption of water molecules from the atmosphere.

Elemental analysis. Elemental chemical analyses for C, N and H were carried out using a FLASHEA1112 (ThermoFinnigan) Analyzer.

For compound **1**: calculated: C: 46.32, H: 5.72, N: 9.53; found: C: 46.53, H: 5.48, N: 9.75. For compound **2**: calculated: C: 48.04, H: 5.07, N: 9.04; found: C: 48.53, H: 5.38, N: 9.30. For compound **3**:

calculated: C: 45.28, H: 5.67, N: 12.18; found: C: 44.32, H: 4.98, N: 11.89. For compound **4**: calculated: C: 51.27, H: 5.41, N: 7.66; found: C: 49.93, H: 5.23, N: 7.49.

Thermal studies. Thermogravimetric analysis (TGA) were carried out in a TGA-DTA Thermal Analysis SDT2960 equipment. For these experiments approximately 25 mg of sample were heated at a rate of 5 K/min from 300 K to 1023 K using corundum crucibles under a flow of dry nitrogen.

Infrared Spectroscopy. Infrared spectra were recorded at room temperature with the FT-IR spectrometer Bruker VECTOR22 over the wavenumber range 400-4000 cm^{-1}.

X-ray diffraction studies. The compounds were studied by X-ray powder diffraction (XRPD) at room temperature in a Siemens D-5000 diffractometer using CuKα radiation (λ=1.5418 Å). The XRPD patterns were analyzed by the Le Bail profile analysis using the Rietica software.[27]

Additionally, in the case of compound **1** (the only compound from which we have obtained crystals that are adequate for single crystal X-ray diffraction) single-crystal data sets were collected at 293 K and 100 K. These experiments were carried out in a Bruker-Nonius x8 ApexII X-ray diffractometer equipped with a CCD detector and using monochromatic MoKα_1 radiation (λ=0.71073 Å). A suitable crystal was chosen and mounted on a glass fiber using instant glue. For the 100 K set, the crystal temperature was maintained using a cold stream of nitrogen from a Kyroflex cryostream cooler. The data integration and reduction was performed using the Apex2 V.1.0-27 (Bruker Nonius, 2005) suite software. The intensity collected was corrected for Lorentz and polarization effects and for absorption by semiempirical methods on the basis of symmetry-equivalent data using SADABS (2004) of the suite software. The structures were solved by the direct method using the SHELXS-97 program[28] and were refined by least squares method on SHELXL-97.[29]

Dielectric properties. The complex dielectric permittivity ($\varepsilon_r = \varepsilon'_r - i\varepsilon''_r$) of these samples was measured as a function of frequency and temperature with a parallel-plate capacitor coupled to a Solartron 1260A Impedance/Gain-Phase Analyzer, capable to measure in the frequency range 10 μHz to 32 MHz. The capacitor was mounted in a Janis SVT200T cryostat refrigerated with liquid nitrogen, and with a Lakeshore 332 incorporated to control the temperature from 100 K up to 350 K.

As the obtained single crystals of 1 were not big enough to perform single crystal dielectric measurements, in all cases pellets made out of well-dried samples were measured instead. This latter aspect is also important as the presence of adsorbed water can greatly interfere in the observed dielectric response.

Such pellets with an area of approximately 300 mm^2 and thickness of approximately 0.6 mm were prepared to fit into the capacitor, and silver paste was painted on their surfaces to ensure a good electrical contact with the electrodes.

All the dielectric measurements were carried out in a nitrogen atmosphere where several cycles of of vacuum and nitrogen gas were performed to ensure that the sample environment is free of water.

The impedance analysis software SMART (Solartron Analytical) was used for data acquisition and processing. Impedance complex plane plots were analyzed using the LEVM program, a particular program for complex nonlinear least squares fitting.[30]

Polarization (P) *vs.* electric field (E) measurements were carried out using a home-built setup based on a Sawyer–Tower circuit where the hysteresis loops were recorded using a Keithley 6517B electrometer.

RESULTS

Characterization

The XRPD patterns show that the obtained samples are single phase materials (Fig. 2). In addition, the structural data obtained from the LeBail refinements are in full agreement with those already reported in the literature.[20] In this context, the compounds **1** and **2** show tetragonal symmetry (S.G.: I4/mcm) and the following cell parameters: a=15.181(1) Å and c=19.085(1) Å for M=Co^{2+} and a=15.127(1) Å and c=18.667(1) Å for M=Ni^{2+}. Therefore, the substitution of the Co^{2+} ion ($^{VI}r_{Co}{}^{2+}$= 0.74 Å)[31] by the relatively smaller Ni^{2+} ion ($^{VI}r_{Ni}{}^{2+}$= 0.69 Å)[31] results in a slight contraction of the corresponding cell parameters, as expected.

As for the closely related compounds **3** and **4**, whose structure had not been published before, the corresponding LeBail refinement indicates that they also show tetragonal symmetry with cell parameters a=15.2649(6) Å and c=19.1212(5) Å (S.G.: I4/mcm) in the case of compound **3**, and a=10.8997(7) Å and c=9.7794(8) Å (S.G.: P4/mmm) in the case of compound **4**.

The structure of compound **1** could also be solved by single crystal X-ray diffraction both at room temperature and at 100 K (see the S.I.: Tables SI and SII and Figs. S2-4). The room temperature structure, that is reported for the first time in this work, presents two major structural differences with respect to that found at low temperature (and that is in agreement with that already described):[25] 1/ the *1,4-bdc* ligand is split into two different possible positions of equal electron density, effect that is not present at 100 K (see S.I. Fig. S4). 2/ At room temperature the guest molecules (DMF and water) seem to be randomly distributed inside the MOF cages and, even if their electron density is clearly detected, a satisfactory refinement including their atomic positions could not be obtained. Meanwhile, at low temperature, the location of these molecules could be established (see S.I. Fig. S3).

On the other hand, at both temperatures the C atoms of the dabco pillars are found to be disordered, as it had already been reported for the low temperature structure (ref).

IR spectra for the four $M_2(L)_2(dabco)\cdot[G]$ compounds are quite similar and in agreement with those reported in the literature for $M_2(1,4\text{-bdc})_2(dabco)\cdot[G]$[23] (see S.I. Fig. S5). The presence of water is clearly detected by the presence of a broad band around 3500 cm^{-1} while the band at 1095 cm^{-1} could be ascribed to the asymmetric stretching vibration of the methyl group of DMF molecules.

A typical TGA curve for these compounds is shown in S.I. Fig S6. Combining the TGA results with elemental analysis data we have estimated the amount of DMF and H_2O present inside the pores of the structures. According to those results the complete chemical formula of these compounds can be written as follows: **1**:$Co_2(1,4\text{-bdc})_2(dabco)\cdot[4DMF\cdot 1H_2O]$, **2**:$Ni_2(1,4\text{-bdc})_2(dabco)\cdot[3DMF\cdot 1/2H_2O]$, **3**: $Co_2(1,4\text{-bdc-}NH_2)_2(dabco)\cdot[7/2DMF\cdot 1H_2O]$ and **4**: $Co_2(1,4\text{-ndc})_2(dabco)\cdot[3DMF\cdot 2H_2O]$.

Moreover TGA results reveal that these compounds are stable up to 373 K. Above this temperature they start to lose H_2O and DMF, to finally decompose around 523 K. [23,25]

As for their stability in air, it should be mentioned that only compound **1** is seen to evolve with time rather quickly, so that it should be handled with care. Meanwhile the rest of the compounds are stable, specially the Ni-one. Therefore, we have chosen compound **2** to carry out further experiments by eliminating the guest molecules.

For this purpose we have heated the as obtained compound **2** at 473 K for 2h, obtaining $Ni_2(1,4\text{-bdc})_2(dabco)$ (compound **5**). The XRPD pattern of **5** reveals that its structural framework basically remains unchanged after this thermal treatment, although there is a slight peak broadening and a shift of the diffraction maxima (see S.I. Fig. S7). Also, in the IR spectrum of this compound the bands from the carboxylate groups and the benzene rings are still present, thus confirming the integrity of the 3D skeleton of the metal organic framework. Meanwhile the disappearance of the broad band around 3500 cm^{-1}, previously detected in compound **2**, corroborates the elimination of the guest H_2O molecules initially located inside the pores (see S.I. Fig. S5).

Dielectric behavior

Figure 3 shows the temperature dependence of the real part of the complex dielectric permittivity ε'_r (the so-called dielectric constant) of pressed pellets of $Co_2(1,4\text{-bdc})_2(dabco)\cdot[4DMF\cdot 1H_2O]$ (compound **1)**. As it can be seen, the dielectric constant goes through a broad and pronounced maximum close to room temperature, giving rise to very large colossal values at 300 K, specially at low measuring frequencies, for example $\varepsilon'_r \approx 5000$ at 300 K for ν= 100 Hz.

The compound **2**, which contains Ni^{2+} instead Co^{2+}, shows a similar behaviour although the increase of its dielectric constant at room temperature is considerably smaller, with values almost two orders of magnitude lower than those observed in compound **1** (see Fig. 4).

In the case of compounds **3** and **4**, their dielectric constant also goes through a small maximum close to room temperature, but with very reduced values compared to those of the compound **1** (see Fig. 5).

If we now compare the behavior of compound **2** (fresh sample) with that of compound **5**, from which the guest molecules have been removed, we can see that the broad peak that is observed in the fresh

sample close to room temperature has completely disappeared, and no anomaly is detected in the dielectric constant, that is very low an temperature independent (see Fig. 4).

To deepen further into the dielectric behavior displayed by these samples, we have carried out impedance spectroscopy studies as a function of frequency and temperature. As it is well-known, this technique is a very powerful tool to unravel the dielectric response of materials[15b] and to avoid misinterpreting results such as apparent hysteresis loops displayed by electrically inhomogeneous samples.[32,33]

The behavior displayed by $Co_2(1,4\text{-bdc})_2(dabco)\cdot[4DMF\cdot 1H_2O]$ (compound **1),** that is again different from the rest, will be presented in first place.

Fig. 6 shows typical impedance complex plane plots for compound **1** in the temperature interval $110 \leq T(K) \leq 260$ (Fig. 6a) and $260 < T(K) \leq 350$ (Fig. 6b). As it can be seen, in the interval $110 \leq T(K) \leq 260$ the corresponding impedance complex plane plots show a single large arc (Fig. 6a), while for T>260 K an additional second small arc appears in the low frequency range (Fig. 6b).

The large arc can be modeled by an equivalent circuit containing three elements connected in parallel: a resistance (R) and a capacitance (C), that is frequency independent, and a frequency-dependent distributed element (DE). As this large arc intercepts zero for T≤260 K and the order of magnitude of its capacitance is of $pFcm^{-1}$ it seems to be associated with the material bulk response.[15b)] The intrinsic dielectric constant (ε'_r) calculated from the value of the obtained capacitance is around 4.6. Taking into account that this is the only contribution present for T≤260 K, the observed dielectric response is purely intrinsic in this low temperature interval.

The second arc observed for T>260 K can be modeled as a single RC connected in series with the circuit that describes the bulk arc. The capacitance of such low frequency arc is about μcm^{-1}, typical of extrinsic contributions such as electrode effects, blocking electrodes, etc.[15b)] This means that in the higher temperature interval, including room temperature, the dielectric response of compound **1** contains both intrinsic and extrinsic contributions.

In this regard, it should be emphasized that while for 110≤T(K)≤260 compound **1** behaves as an insulator ($\sigma<10^{-9}$ S/cm for T<260 K), for T>260 K it becomes semiconducting (i.e. σ~0. 5 μS/cm for T= 320 K).

These results, together with the very large values of the dielectric constant measured for T>260 K at low frequencies, signal the activation of interfacial polarization effects in the $Co_2(1,4\text{-bdc})_2(dabco)\cdot[4DMF\cdot 1H_2O]$ compound close to room temperature.

Meanwhile, in the case of compounds **3**, **4** and **5**, in the whole temperature interval studied, the impedance complex plane plots only show a large single arc that intercepts zero, and the samples remain insulating even at room temperature (see S.I. Fig. S8a). This result implies that the dielectric response of these compounds **3-5** is purely intrinsic.

Finally, the impedance complex plane plots of compound **2** in the temperature interval 260<T(K)≤.350 K reveal a scenario that seems intermediate between the two presented above. They show a large single large arc (see S.I. Fig. S8b), that can be equally well modeled on the basis of two different equivalent circuits: the first one typical for a purely intrinsic response (containing three elements connected in parallel R, C and DE) and the second one typical for the coexistence of extrinsic and intrinsic contributions (containing a single RC connected in series with the circuit that describes the intrinsic response). And the agreement factors do not give a clear advantage of one over the other, so that the situation seems to be intermediate between the two. These results, together with the relative large values of the dielectric constant measured at T>260 K at low frequencies, point towards the presence of interfacial polarization effects in $Ni_2(1,4\text{-bdc})_2(dabco)\cdot[4DMF\cdot 1H_2O]$, even if their contribution is smaller than in the case of compound **1**.

DISCUSSION

The chemical characterization of the obtained samples fully confirms that we have obtained the desired porous hybrid materials $M_2(L)_2(dabco)\cdot[G]$ ($M=Co^{2+}$, Ni^{2+} and L= *1,4-bdc, 1,4-bdc-*NH_2*, 1,4-ndc*) as single phase pure materials. Evenmore, starting from $Ni_2(1,4\text{-bdc})_2(dabco)\cdot[3DMF\cdot 1/2H_2O]$ we

have been able to progressively eliminate the guest molecules from the cavities while retaining the integrity of the 3D structural skeleton.

The obtained hybrid compounds $M_2(L)_2(dabco)\cdot[G]$ ($M=Co^{2+}$, Ni^{2+} and L= *1,4-bdc*, 1,*4-bdc-NH2*, *1,4-ndc*) show a maximum in their $\varepsilon'_r(T)$ curves around 300 K, that in the case of $Co_2(1,4\text{-bdc})_2(dabco)\cdot[4DMF\cdot 1H_2O]$ gives rise to a very large (colossal) dielectric constant at room temperature.

Very interestingly, the appearance of such a maximum of ε'_r around 300 K is related to the presence of the guest molecules located inside the cavities, as the elimination of those molecules results in its disappearance. As the dielectric constant of H_2O is known to exhibit an abrupt jump from 273 K,[8] in principle the appearance of this peak seems to be related to changes in the polarizability of the H_2O molecules confined in the cavities. The interaction of those H_2O molecules with DMF, or even with the framework, could slightly broad and shift the peak toward higher temperatures.[34]

But what it is indeed remarkable is the elevated values of the dielectric constant displayed by compound **1**, much higher than those corresponding to pure H_2O ($\varepsilon'_r \approx 88$) or to DMF ($\varepsilon'_r \approx 38$).

Impedance spectroscopy studies are most revealing in this context: they unambiguously show that such very high dielectric constant is not purely intrinsic, but is greatly enhanced by the activation of extrinsic dielectric effects close to room temperature. When such extrinsic contributions disappear, the dielectric constant values turn to be much smaller, as observed in the case of compounds **3** and **4**.

With all this information in hand, we attribute the intrinsic dielectric response of these materials to the presence of dipolar guest molecules inside the cavities and to their concomitant orientational polarizability. This latter will be small at low temperatures when the guest molecules are frozen in specific positions with very reduced thermal motion. Nevertheless, their degree of freedom will markedly increase with temperature, resulting in a higher polarizability close to room temperature.

As for the origin of the extrinsic effects, that magnify the intrinsic response and that in the case of compound **1** give rise to a colossal dielectric constant, our explanation is the following: we relate it to the characteristics of the porous structure and to the presence of the guest molecules.

In the Co-compound the "medium" size 3D interconnected pore system inside its framework presents relatively wide open channels (of pore diameter 7.6 x 7.6 Å along the c-axis intersected by smaller channels of 3.7 x 5.1 Å along the a and b axis) and recent molecular dynamic simulations have shown that small molecules can diffuse through them.[35] Should this occur with the H_2O and DMF species, an almost liquid-like state would be present throughout the skeleton framework, which could be readily polarized in the presence of an electric field. This effect could also account for the increase in the electrical conductivity that is observed above 260 K, and that finally gives rise to the appearance of extrinsic effects associated to the formation of an electrical double layer at the electrodes.

If we prevent such diffusion from occurring the extrinsic contribution will disappear, the dielectric response will turn out to be purely intrinsic and the magnitude of the $\varepsilon'_r(T)$ maximum will substantially decrease.

This is in fact what is observed in samples **3** and **4**, where such extrinsic contribution is totally eliminated by blocking the channel´s window, so that the guest molecules can no longer diffuse. As a result, the dielectric response is purely intrinsic and the dielectric constant small ($\varepsilon'_r \approx 6$ at 300 K for ν=1000 Hz).

Meanwhile in the case of compound **2**, the extrinsic contribution is only partially eliminated by reducing the size of the cavities, so that a small diffusion can still occur. This results in a small enhancement of the dielectric constant at room temperature, that achieves higher values than in the case of compounds **3** and **4** ($\varepsilon'_r \approx 150$ at 300 K for ν=100 Hz), even if they are much smaller than those of compound **1**.

Very importantly, extrinsic contributions are going to be present in the dielectric response of any porous MOF that presents a certain conductivity; most probably in the CDC porous MOFs cited in the introduction of this paper whose structures are open enough to allow the long range migration of the guest molecules through their channels.

All these extrinsic effects need to be taken into account to adequately describe the dielectric behaviour of MOF samples avoiding, among others, the misinterpretation of closed P(E) curves

measured on such systems (see S.I. Fig. S9, that shows the apparent P(E) curve displayed by compound **1**). If not, we would just be repeating the errors that gave rise to the celebrated and extremely critical viewpoint articles "Ferroelectrics go bananas" [32] and "Bananas go paraelectric" [33] written in view of the proliferation of errors in the papers published in those days in the context of oxides with magneoelectric multiferroic behavior.

CONCLUSIONS

In conclusion, we have shown that the hybrid material $Co_2(1,4\text{-bdc})_2(dabco)\cdot[4DMF\cdot 1H_2O]$, shows a colossal dielectric constant at room temperature ($\varepsilon'_r \approx 5000$ at 300 K for ν=100 Hz). We attribute these colossal values to an order-disorder process of the dipolar guest molecules allocated in the cavities of the framework structure, that is further enhanced by the activation of extrinsic interfacial polarization effects in that temperature window associated to the diffusion of numerous guest molecules through the channels and the formation of the concomitant electrical double layer.

Therefore, it is an apparent colossal dielectric behavior that does not imply colossal polarizability processes, as the dielectric constant is not purely intrinsic, but is greatly enhanced by the activation of extrinsic dielectric effects close to room temperature. If such extrinsic contributions are eliminated or reduced, the values of the dielectric constant turn to be much smaller, as observed in the closely related compounds $Co_2(1,4\text{-bdc-}NH_2)_2(dabco)\cdot[7/2DMF\cdot 1H_2O]$, $Co_2(1,4\text{-ndc})_2(dabco)\cdot[3DMF\cdot 2H_2O]$ and $Ni_2(1,4\text{-bdc})_2(dabco)\cdot[3DMF\cdot 1/2H_2O]$.

On this basis, we identify the basic "ingredient" that is present in MOF materials with apparent CDC constants: a certain conductivity that can arise from diffusion of guest molecules through the channels.

Therefore, we warn about the imperious necessity of distinguishing between intrinsic and extrinsic effects in electrically inhomogenous MOF materials that display a certain conductivity in order to adequately interpret their dielectric behavior.

ACKNOWLEDGEMENTS

The authors are grateful for financial support from Ministerio de Economía y competitividad (Spain) under project FEDER MAT2010-21342-C02-01 and from Xunta de Galicia under project PGIDIT10PXB103272PR.

Supporting Information Available:

Single crystal X-ray diffraction information and structure views of the $Co_2(1,4\text{-bdc})_2(dabco)\cdot[G]$ compound at different temperatures (100 K and 293 K). Infrared spectra of compounds **2** and **5**. TGA analysis of compound 2. XRPD pattern at room temperature of compounds **2** and **5**. Typical impedance complex plane of compounds **2** and **4**. "Apparent" P(E) hysteresis loop of the compound **1**. This material is available free of charge via the Internet at http://pubs.acs.org.

REFERENCES

1 (a) Yaghi, O. M.; O'Keeffe, M.; Ockwig, N. W.; Chae, H. K.; Eddaoudi, M.; Kim, J. *Nature* **2003**, *423*, 705-714. (b) Fletcher, A. J.; Thomas, K. M.; Rosseinsky, M. J. *J. Solid State Chem*. **2005**, *178*, 2491-2510.

2 (a) Cheetham, A.K.; Rao C.N.R. *Science* **2007**, *318*, 58-59. (b) Ferey, G. *Chem. Soc. Rev.* **2008**, *37*, 191-214. (c) Rogez, G.; Viart, N.; Drillon, M. Angew. *Chem. Int. Ed*. **2010**, *49*, 1921-1923.

3 (a) Guo, M.; Cai, H. L.; Xiong, R. G. *Inorg. Chem. Comm.* **2010**, *13*, 1590-1598. (b) Hang, T.; Ye. H. Y.; Xiong, R. G. *Chem. Soc. Rev.* **2011**, *40*, 3577-3598. (and ref. therein).

4 Xu, G. C.; Zhang, W.; Ma X. M.; Chen, Y. H.; Zhang, L.; Cai, H. L.; Wang, Z. M.; Xiong, R. X.; Song Gao, S. *J. Am. Chem. Soc.*, **2011**, *133*, 14948-14951.

5 Jain, P.; Ramachandran, V.; Clark, R. J.; Zhou, H. D.; Toby, B. H.; Dalal, N. S.; Kroto, H. W.; Cheetham, A. K. *J. Am. Chem. Soc.* **2009**, *131*, 13625-13627.

6 (a) Jain, P.; Dalal, N.S.; Toby, B. H.; Kroto, H. W.; Cheetham, A.K. *J. Am. Chem. Soc.* **2008**, *130*, 10450-10451. (b) Sánchez-Andújar, M.; Presedo, S.; Yáñez-Vilar, S.; Castro-García, S.; Shamir, J.; Señarís-Rodríguez, M. A. *Inorg. Chem.* **2010**, *49*, 1510-1516. (c) Besara, T.; Jain, P.; Dalal, N. S.; Kuhns, P.L.; Reyes, A. P.; Kroto, H. W.; Cheetham, A. K. *Proc. Natl. Acad. Sci.* **2011**, *108*, 6828-6832. (d) Fu, A. W.; Zhang, W.; Cai, H.L.; Zhang, Y.; Ge, J.Z.; Xiong. R.G.; Huang, S.D.; Nakamura,T. *Angew. Chem. Int. Ed.* **2011**, *50*, 11947-11951.

7 Xu, G. C.; Ma, X. M.; Zhang, L.; Wang, Z. M.; Gao. S. *J. Am. Chem. Soc.* **2010**, *132*, 9588-9590.

8 Cui, H.; Takahashi, K.; Okano, Y.; Kobayashi, H.; Wang, Z.; Kobayashi, A. *Angew. Chem. Int. Ed.* **2005**, *44*, 6508-6512.

9 Cui, H.; Wang, Z.; Takahashi, K.; Okano, Y.; Kobayashi, H.; Kobayashi, A. *J. Am. Chem. Soc.* **2006**, *128*, 1507-1510.

10 Cui, H.; Zhou, B.; Long, L. S.; Okano, Y.; Kobayashi, H.; Kobayashi, A. *Angew. Chem. Int. Ed.* **2008**, *47*, 3376-3380.

11 Zhou, B.; Kobayashi, A.; Cui, H.; Long, L.; Fujimori, H.; Kobayashi, H. *J. Am. Chem. Soc.* **2011**, *133*, 5736-5739.

12 Penafiel, L. M; Litovitz, T. A. *J. Chem. Phys.* **1992**, *97*, 559-567.

13 Ji, W. J.; Zhai, Q. G.; Li, S-N.; Jiang, Y. C.; Hu, M. C. *Chem. Comm.* **2011**, *47*, 3834-3836.

14 Lunkenheimer, P.; Krohns, S.; Riegg, S.; Ebbinghaus, S.G.; Reller, A.; Loidl, A. *European Physical Journal* **2009**, *180*, 61-89.

15 (a) Lunkenheimer, P.; Bobnar, V.; Pronin, A. V.; Ritus, A. I.; Volkov, A.; Loild, A. *Phys. Rev. B.* **2002**, *66*, 052105/1-052105/4. (b) Sinclair, D. C.; Adams, T. B.; Morrison, F. D.; West, A. R. *Appl. Phys. Lett.* **2002**, 2153-2155. *80*

16 Subramanian, M. A.; Dong, L.; Duan, N.; Reisner, B. A.; Sleight, A. W. *J. Solid State Chem.* **2000**, *151*, 323-325.

17 Homes, C.C.; Vogt, T.; Shapiro, M.; Wakimoto, S.; Ramírez, A. P. *Science* **2001**, *293*, 673-676.

18 Castro-Couceiro, A.; Yáñez-Vilar, S.; Sánchez-Andujar, M.; Rivas-Murias, B.; Rivas, J.; Señarís-Rodríguez, M.A. *Prog. Solid State Chem.* **2007**, *35*, 379-386.

19 Von Hippel, A. *Dielectrics and Waves*, Artech House: Boston, 1995.

20 Schwan, H. P. *Interaction Mechanisms of Low-Level Electromagnetic Fields in Living Systems*, Oxford University Press: *Oxford*, 1992.

21 Moulson, A. J.; Herbert, J. M. *Electroceramics: Materials, Properties, Applications*, John Wiley & Sons: West Sussex, 2003.

22 Simon, P.; Gogotsi, Y. *Nature Mat.* **2008**, *7*, 845-854.

23 (a) Z. Liang, M. Marshall, A. L. Chaffee, *Micropor. Mesopor. Mat.* **2010**, *132*, 305-310. (b) B. Arstad, H. Fjellvag, K. O. Kongshaug, O. Swang, R. Blom, *Adsorption* **2008**, *14*, 755-762.

24 Dybtsev, D.N.; Chun, H.; Kim, K. *Angew Chem. Int. Ed.*, **2004**, *43*, 5033-5036.

25 Wang, H.; Getzschmann, J.; Senkovska, I.; Kaskel, S. *Micropor. Mesopor. Mat.* **2008**, *116*, 653-657.

26 Chun, H.; Dybtsev, D. N.; Kim, H.; Kim, K. *Chem. Eur. J.* **2005**, *11*, 3521-3529.

27 Howard, C. J.; Hunter, H.; Rietica, B. A. *A Computer Program for Rietveld Analysis of X-ray and Neutron Podwer Diffraction Patterns*, Australian Nuclear Science and Technology Organization Lucas Heights Research Laboratories.

28 Sheldrick, G. M. *SHELXS-97: Program for Crystal Structure Resolution*; University of Göttingen: Göttingen, Germany, 1997.

29 Sheldrick, G. M. *SHELXL-97: Program for Crystal Structure Analysis;* University of Göttingen: Göttingen, Germany, 1997.

30 J. Ross Macdonald, *LEVM version 8.0 Comlex Nonlinear Squares Fitting Program*, 2003.

31 R.D. Shannon, C.T. Prewitt, *Acta Cryst. B* **1969**, *25*, 925-945.

32 Loidl, A.; Krohns, S.; Hemberger J.; Lunkenheimer, P. *J. Phys.: Condens. Matter* **2008**, *20*, 19100.

33 Scott, J. F. *J. Phys.: Condens. Matter* **2008**, *20*, 21001.

34 Jia, G.Z.; Huang, K.M.; Yang L.J.; Yang, X.Q. *Int. J. Mol. Sci.* **2009**, *10*, 1590-1600.

35 Krishna, R. *J. Phys. Chem. C* **2009**, *113*, 19756-19781.

FIGURE CAPTIONS

Figure 1. Crystal structure of $M_2(1,4\text{-bdc})_2(dabco)\cdot[G]$ (M: Co^{2+}, Ni^{2+}) at low temperature (T=100 K?) The carbon atoms of *dabco* pillars are disordered.

Figure 2. Room temperature XRPD pattern of: a) compound **1**, b) compound **2**, c) compound **3** and d) compound **4**.

Figure 3. Temperature dependence of the dielectric constant of compound **1** measured at different frequencies in the temperature interval 100<T(K)<350.

Figure 4. Dielectric constant (a) and loss tangent (b) of the compounds **2** and **5** in the temperature interval 100<T(K)<350 (measuring frequency ν=100Hz).

Figure 5. Comparison of the dielectric constant (a) and loss tangent (b) of $[Co_2(L)_2(dabco)]\cdot[G]$ compounds with different ligands L: *1,4-bdc* (compound **1**), *1,4-bdc-NH_2* (compound **3**) and *1,4-ndc* (compound **4**), in the temperature interval 100<T(K)<350 and measuring frequency ν=1000 Hz.

Figure 6. Typical impedance complex plane of compound **1** in the temperature range a) $110 \leq T\,(K) \leq 260$ and b) $260 < T\,(K) \leq 350$.

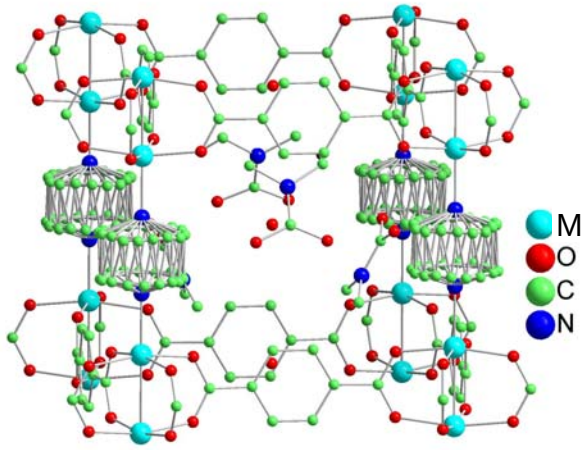

Figure 1

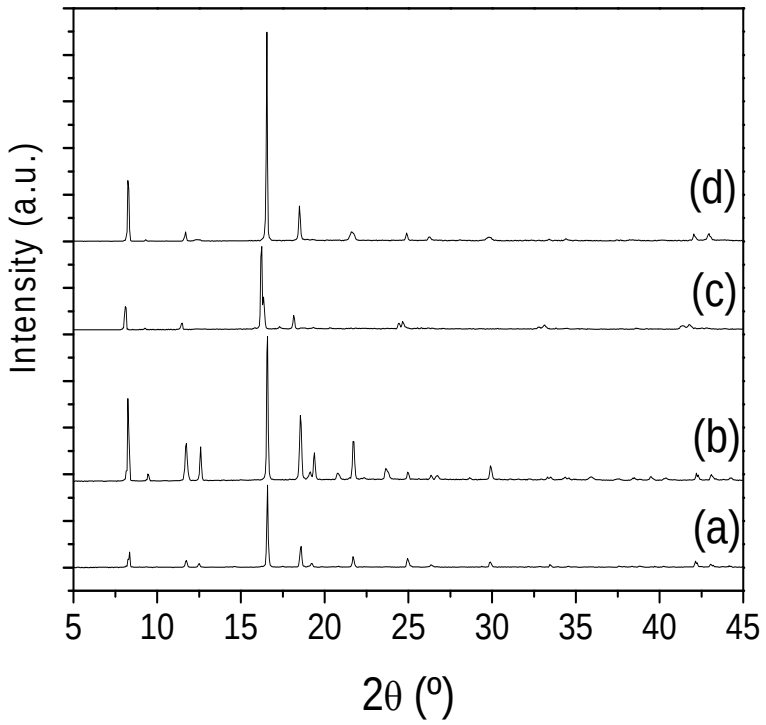

Figure 2

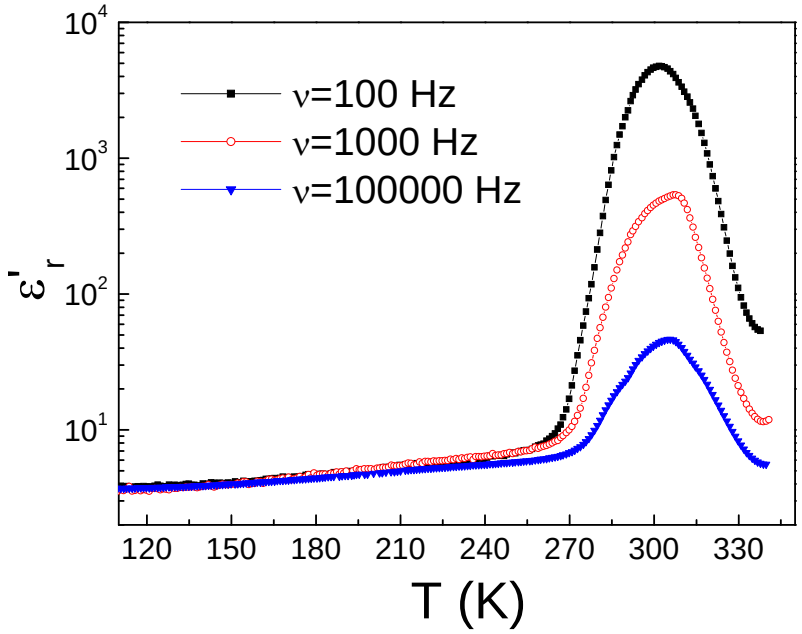
ν=100 Hz
ν=1000 Hz
ν=100000 Hz
ε'r
T (K)
10^4
10^3
10^2
10^1
120
150
180
210
240
270
300
330

Figure 3

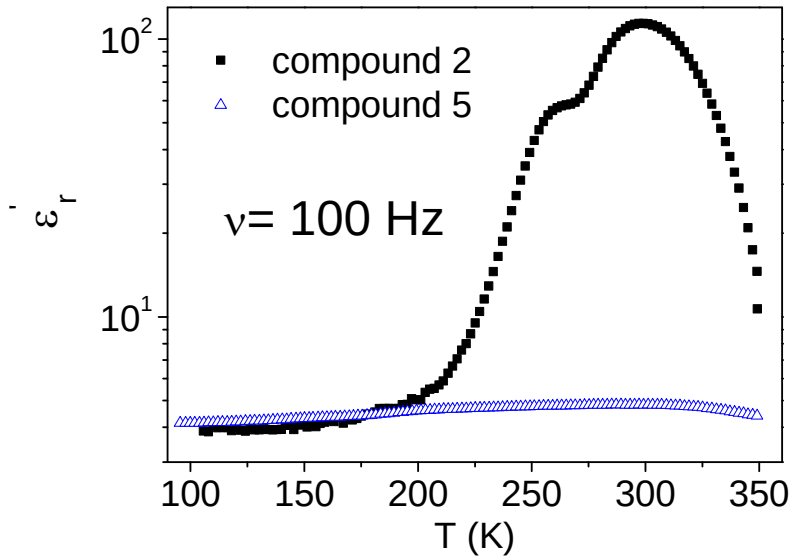

A)

y poner debajo loss tangent como b)

Figure 4

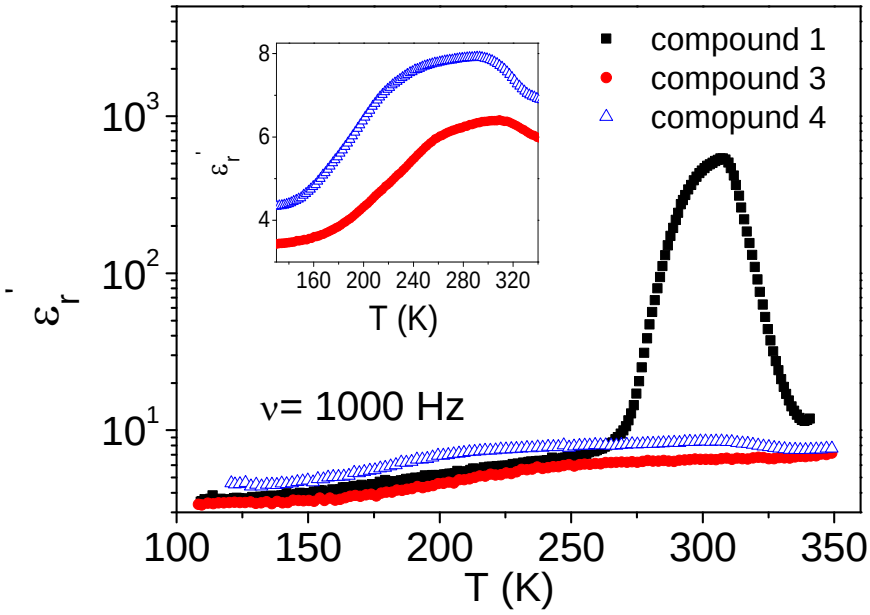

Figure 5

a) y poner debajo loss tangent como b)

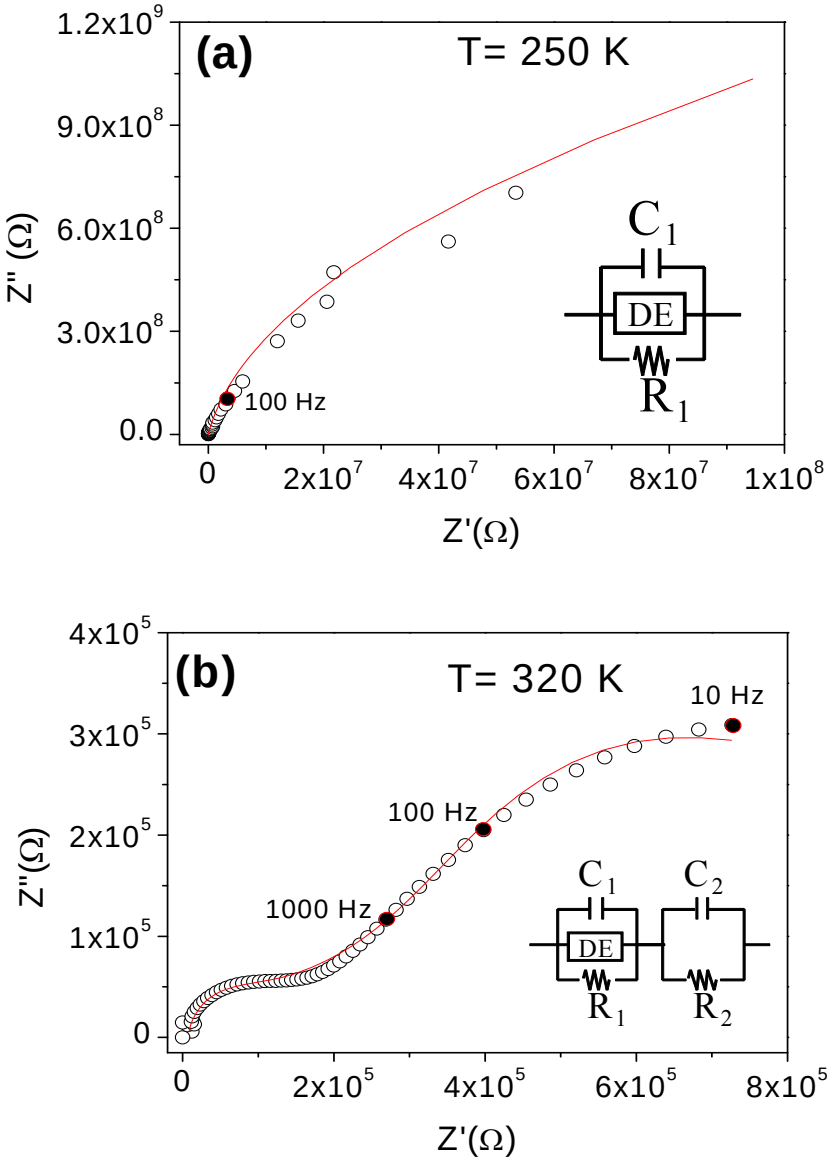
(a)
T= 250 K
100 Hz
C1
DE
R1
Z'' (Ω)
Z'(Ω)
1.2x10^9
9.0x10^8
6.0x10^8
3.0x10^8
0.0
0
2x10^7
4x10^7
6x10^7
8x10^7
1x10^8
(b)
T= 320 K
10 Hz
100 Hz
1000 Hz
C1
C2
DE
R1
R2
Z''(Ω)
Z'(Ω)
4x10^5
3x10^5
2x10^5
1x10^5
0
0
2x10^5
4x10^5
6x10^5
8x10^5

Figure 6

TOC

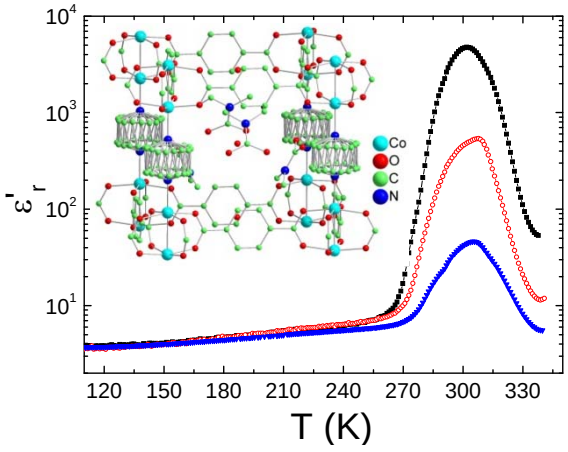
10^4
10^3
10^2
10^1
ε'_r
Co
O
C
N
120
150
180
210
240
270
300
330
T (K)